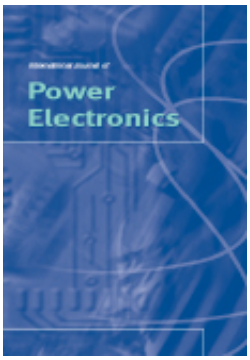

International Journal of Power Electronics

ISSN online: 1756-6398 - ISSN print: 1756-638X
https://www.inderscience.com/ijpelec

A study on attraction type electromagnetic levitation systems for four different shaped objects

Janardan Kundu

DOI: 10.1504/IJPELEC.2024.10057096

Article History:

Received:	12 October 2022
Last revised:	24 January 2023
Accepted:	13 February 2023
Published online:	23 December 2023

A study on attraction type electromagnetic levitation systems for four different shaped objects

Janardan Kundu

Department of Electrical Engineering,
University College of Engineering and Technology,
Karni Industrial Area, Pugal Road,
Bikaner, Rajasthan – 334004, India
Email: janardan.netaji@gmail.com

Abstract: This paper highlights the system dynamics during sustained oscillation in x-direction and a brief comparative study of levitation systems for a steel ball (62 gm), two steel plates (65 gm and 148 gm) and a C-shaped steel plate (148 gm). The dynamics, e.g., force, inductance, velocity, acceleration, restoring force, current, etc., due to disturbance in x-direction has been obtained for four different shaped objects. The nature of stable equilibrium point at the operating point has been observed closely for different shaped and dimensions-based levitation systems. Currently, maglev trains are being run on a limited basis in Germany and Japan. In real transportation problems, the geometric discontinuity of the platform is of special interest. The effects of perturbations in x-direction for asymmetric objects has been broadly investigated in this work and has been compared with a symmetric object.

Keywords: electromagnetic levitation; lead compensator; window comparator; frequency analysis.

Reference to this paper should be made as follows: Kundu, J. (2024) 'A study on attraction type electromagnetic levitation systems for four different shaped objects', *Int. J. Power Electronics*, Vol. 19, No. 1, pp.79–98.

Biographical notes: Janardan Kundu completed his Post-Graduation in Control Systems from the MNNIT Allahabad, India in 2012. In 2013 he joined as a CSIR Senior Research Fellow, Goverment of India at Indian Institute of Engineering Science and Technology, Shibpur. His research areas are control systems, optimal control, adaptive control, etc.

1 Introduction

Maglev (*magnetic levitation*) popularly refers to a system of transport that uses magnetic levitation to suspend, guide, and drive vehicles with the help of magnets without the use of mechanical elements such as wheels, axes, and bearings (Bittar et al., 1998; Jayawant, 1988; Kundu et al., 2013). Here are few other applications of electromagnetic suspension

type levitation in wind tunnel, magnetic bearing, wafer transportation, vibration isolation in sensitive equipment, suspension of molten metal in induction furnaces, etc. (Moon, 1994; Pal et al., 2002; Rogg, 1984; Sengupta and Sengupta, 2001; Sinha, 1987). There are also applications in the semiconductor and biomedical industries. With the help of maglev a vehicle is levitated just above the guideway to create both lift and thrust using magnets or magnetic fields. In the upcoming generation high-speed maglev vehicles can bring a striking improvements in human civilisation in terms of its comfortableness and saving of time in a surprising manner (Yamamura and Yamaguchi, 1990; Chen and Tsukamoto, 1991). In propulsion applications, the energy required for levitation is usually not a large percentage of the total energy consumption (Matsumura and Yamada, 1974; Banerjee et al., 2008; Ohtsuka and Kyotani, 1975; Kundu and Sengupta, 2015; Kundu et al., 2014; Banerjee and Bhaduri, 2010; Wong, 1986). Use of levitation in applications, e.g., magnetic bearings, magnetically lifted trains, etc. has drawn a huge attention throughout worldwide research (Venkataratnam et al., 1998; Jinhui et al., 2015; Mofushita et al., 1989; Ma et al., 2018; Morishita and Azukizawa, 1988; Jo et al., 2010).

Figure 1 Four steel objects of different masses but same geometries and same geometries but with different masses, (a) steel ball (62 gm) (b) rectangular shaped flat steel plate I (65 gm) (c) rectangular shaped flat steel plate II (148 gm) (d) C-shaped steel plate (148 gm) (see online version for colours)

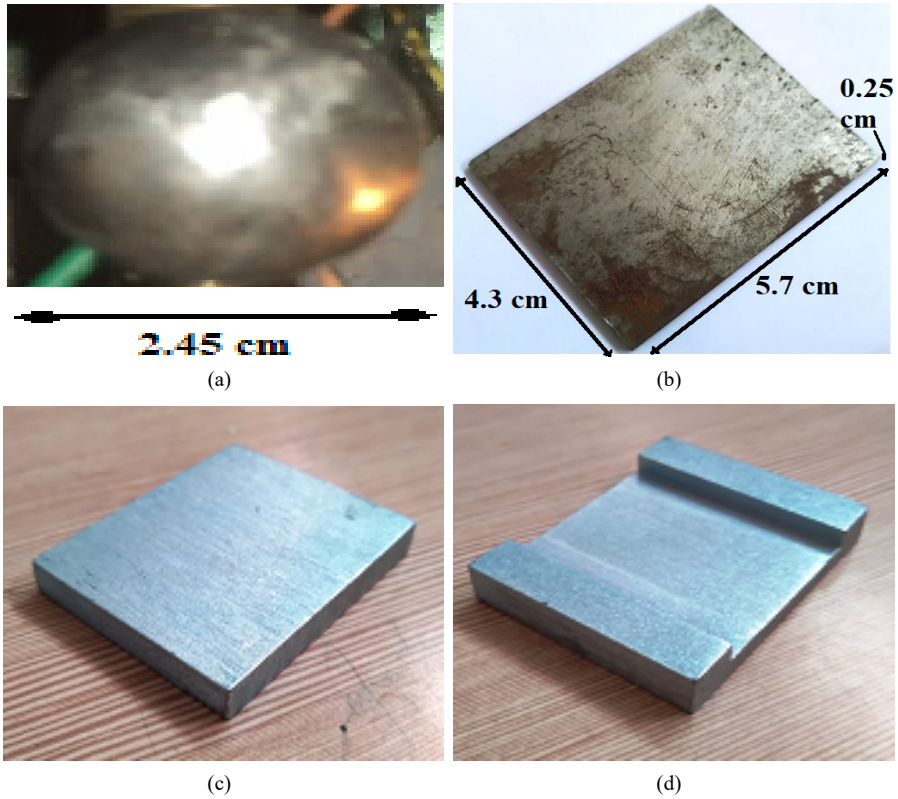

(a) (b)

(c) (d)

A novel servo-stabilised electromagnetic levitation for micro-EDM processing and its feasibility analysis has been discussed by Kumar et al. (2022). Xu et al. (2022) have studied on a novel servo-stabilised electromagnetic levitation for micro-EDM processing and its feasibility analysis. Single-electromagnet levitation for density measurement and defect detection has been studied by Jia et al. (2021). Wang et al. (2020) have studied on dynamic interaction analysis of bridges induced by a low-to-medium-speed maglev train. Sun et al. (2019) have highlighted on fuzzy H_∞ robust control for magnetic levitation system of maglev vehicles based on TS fuzzy model: design and experiments. Wang et al. (2018) have studied on levitation control of permanent magnet electromagnetic hybrid suspension maglev train has been highlighted in Debnath et al. (2018). Nonlinear dynamic modelling and fuzzy sliding-mode controlling of electromagnetic levitation system of low-speed maglev train has been discussed by Sun et al. (2017).

Figure 2 Electromagnetic levitation system for objects of different masses and geometries, (a) ball (b) plate 1 (c) plate 2 (d) C-shaped plate (see online version for colours)

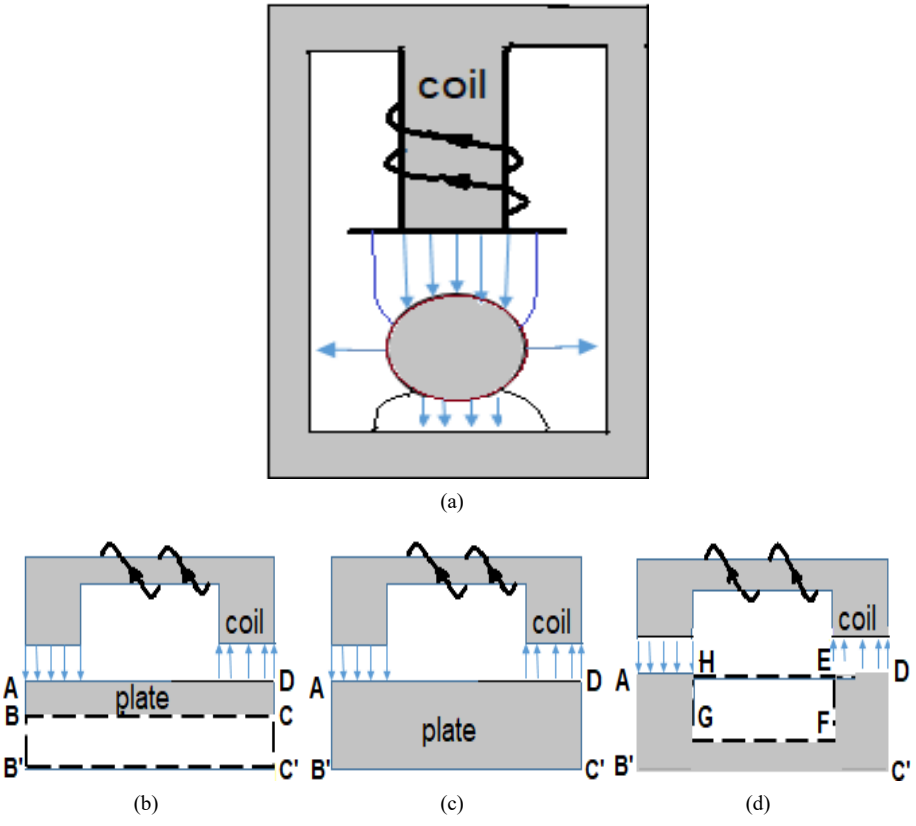

But most interestingly x-direction modelling is totally overlooked in the field of electromagnetic levitation. System dynamics in x-direction and considering it in modelling is a significant contribution and a challenging work has been discussed in this paper. The velocity, acceleration and restoring force plays a substantial and major role to come in a conclusive decision of how much small perturbation a specific levitation system can handle.

This paper studies on an exhaustive comparative study on the system dynamics due to oscillating condition in restoring zone for the displacement in x-direction of four different shaped objects (Figure 1). Velocity, acceleration and restoring force in sustained oscillation during stable levitation has been discussed broadly (Figures 9 and 11). The inductance, $\left(\frac{dL}{dx}\right)$, current (i_x) and restoring force due to the disturbance in x-direction has been shown in Figures 8 and 10. The velocity term in the x-direction, $\left(\frac{dx}{dt}\right)$ have been considered in x-direction modelling. Average model and perturbed model has been highlighted. Inductance behaviour during sustained oscillation has been observed closely. This work will allow the designer to compute the model geometric dimensions with greater accuracy than allowed by the approaches found in the available published literatures.

2 System description

Referring Figure 3, the instantaneous flux linkage across the magnet coil in dynamic condition can be written as,

$$\psi = Li = N\phi \tag{1}$$

Figure 3 Schematic diagram (2D) of a generalised electromagnetic levitation system (front view) (see online version for colours)

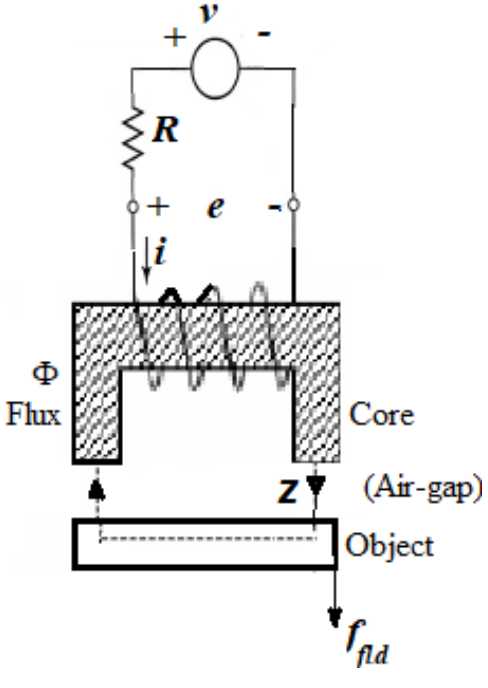

Considering Faraday's law, electromotive force is,

$$\oint_l E.dl = -\frac{d\phi}{dt}$$

Figure 4 3D diagram of an electromagnetic levitation system (see online version for colours)

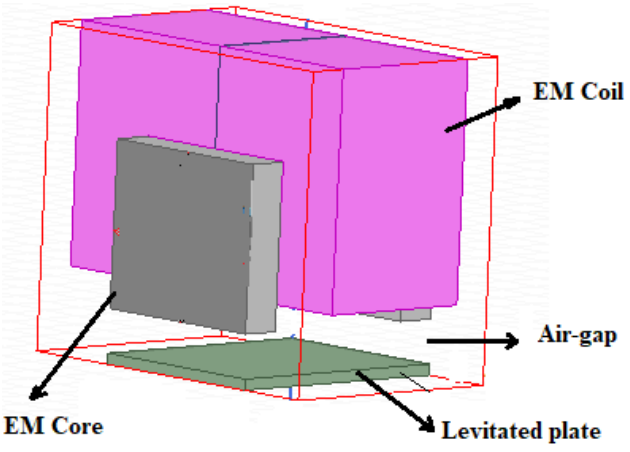

So, the instantaneous voltage across the magnet coil can be expressed as,

$$v = Ri + \frac{d\psi}{dt} \tag{2}$$

Now, considering Ampere's law taken around the core and defining a loop which passes along the centre of the core to form a circle with circumferences l.

$$\oint_l H.dl = \oint_s J.ds$$

In the case where currents are confirmed to wires, each carrying I, the right hand side can be written as NI, where N is the number of wires passing through the contour integral loop. The NI term can be taken as a kind of source equivalent to $H.dl$ The terms $H.dl$ and NI are magnetomotive force (MMF). The left hand side can be split into an integral within the core material plus an integral within the air gap. Assuming that H is nearly uniform in each material, the integrals give $H_{core}l_{core} + H_{air}l_{air}$ for the total $\oint_l H.dl$.

$$H_{core}l_{core} + H_{air}l_{air} = Ni \tag{3}$$

where $B = \mu H$. So the above equation becomes,

$$\frac{B_{core}}{\mu_{core}}l_{core} + \frac{B_{air}}{\mu_{air}}l_{air} = Ni \tag{4}$$

Now, Gauss's law for magnetic fields provide another relationship. Since a given surface s has a magneic flux $\phi = \oint_s B.ds$. If B does not change much then $\phi = \int B.ds = BA$, where A is the cross sectional core area. Then,

$$\frac{\phi_{core}l_{core}}{\mu_{core}A_{core}} + \frac{\phi_{air}l_{air}}{\mu_{air}A_{air}} = Ni \tag{5}$$

Figure 5 Equivalent magnetic circuit of a levitation system

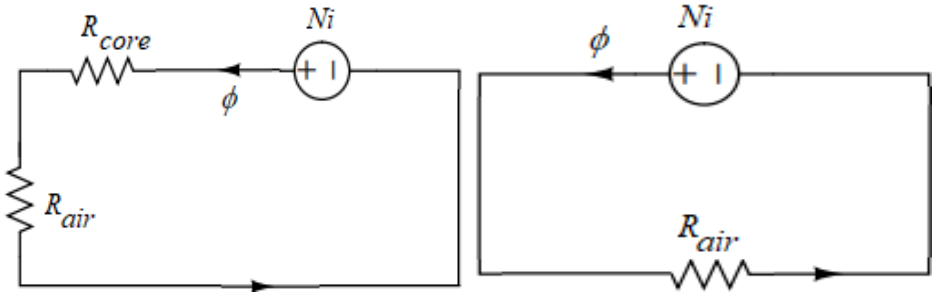

Figure 6 Spatial plots of B vectors for different geometries, (a) spatial plot of B vectors of the ball levitation prototype (FEM-simulated) (b) spatial plot of B vectors of the flat plate levitation prototype (FEM-simulated) (c) spatial plot of B vectors of the C-shaped plate levitation prototype (FEM-simulated) (see online version for colours)

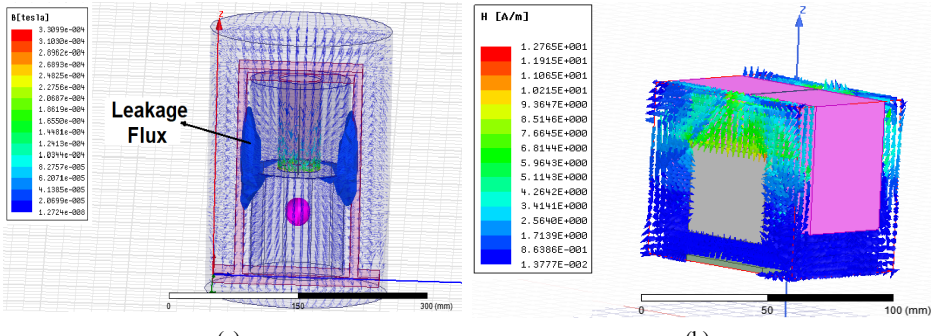

The quantity $\frac{l}{\mu A}$ must be analogous to resistance. For a magnetic circuit, this quantity is called reluctance.

$$\phi_{core}\mathcal{R}_{core} + \phi_{air}\mathcal{R}_{air} = Ni \tag{6}$$

Considering, uniform flux-density in the gap and no leakage of flux $\phi_{core} = \phi_{air} = \phi$

$$\phi(\mathcal{R}_{core} + \mathcal{R}_{air}) = Ni \tag{7}$$

and assuming that the core is unsaturated then $\mathcal{R}_{air} >> \mathcal{R}_{core}$.

So, neglecting $\mathcal{R}_{core}$, the instantaneous coil inductance is written as,

$$L(x,z) = \frac{N}{i}\Phi_T = \frac{N^2}{\mathcal{R}_{air}} = (N^2 \times \mathcal{P}_{air}) \tag{8}$$

Initially as a first case study, a spherical geometry has been studied [Figure 2(a)] and then a flat plate of the same mass [ABCD in Figure 2(b)] has been investigated. Then as a third case study, another flat plate of different mass but same aspect ratio [AB′C′D in Figure 2(b)] has been considered and finally as a forth case study, a C-shaped plate (Figure 2(c)) has been studied where the reluctance force due to its slotting portion (EFGH) plays a significant role in electromagnetic levitation (*EMLS*).

In the ball levitation system [Figure 2(a)], a ferromagnetic guide-way with *EM* coil having I type core has been chosen (for sake of providing a closed magnetic path). Hence, ferromagnetic guide-way will effect on the performance of the *EMLS* (corresponding B plot shown in Figure 6(a), highlighting more flux leakage due to the ferromagnetic guide-way). Hence the leakage is more for the ball levitation set-up whereas an aluminium-made guide-way has been used for the asymmetric shaped plates. Also a C type *EM*-coil has been used for the plate set-ups resulting in almost zero flux leakage [corresponding B plots are shown in Figures 6(b) and 6(c)]. So for the asymmetric shaped plates, the performance is not affected by the ferromagnetic guide-way. But more precise and spirit level accuracy setups are required for the levitation of plates [Figures 2(b) and 2(c)]. The next section studies on the system dynamics in transverse direction.

3 System dynamics in transverse direction

The flux linkages is given by,

$$\psi = Li = N\phi \tag{9}$$

The instantaneous voltage can be written as,

$$v = Ri + \frac{d\psi}{dt} \tag{10}$$

So, the voltage across the electromagnetic coil is expressed as,

$$v = Ri + L\frac{di}{dt} + i\frac{dL}{dt} \tag{11}$$

where L is a function of x and z. Using partial derivative $\frac{dL}{dt}$ can be further divided in two terms, e.g., $\frac{dz}{dt}$ and $\frac{dx}{dt}$ where $\frac{dz}{dt}$ is the velocity (v_z) in z-direction and $\frac{dx}{dt}$ is the velocity (v_x) in x-direction respectively.

$$\text{or, } v = Ri + L\frac{di}{dt} + i\frac{\delta L}{\delta z}\frac{dz}{dt} + i\frac{\delta L}{\delta x}\frac{dx}{dt} \tag{12}$$

$$\text{or, } v = Ri + L(x,z)\frac{di}{dt} + i\frac{\delta L}{\delta x}v_x + i\frac{\delta L}{\delta z}v_z \tag{13}$$

$\frac{\delta L}{\delta z}$ and $\frac{\delta L}{\delta x}$ has been evaluated analytically. Now,

$$\frac{\delta L}{\delta z} = -\frac{N^2 \mu_0 w}{2}\left[\frac{a}{z^2} + \frac{b\beta}{2z^2 + b\beta z}\right] \tag{14}$$

$$\frac{\delta L}{\delta x} = [b + 2cx] \tag{15}$$

where b and c are constant.

Figure 7 Schematic diagram of ball levitation system (see online version for colours)

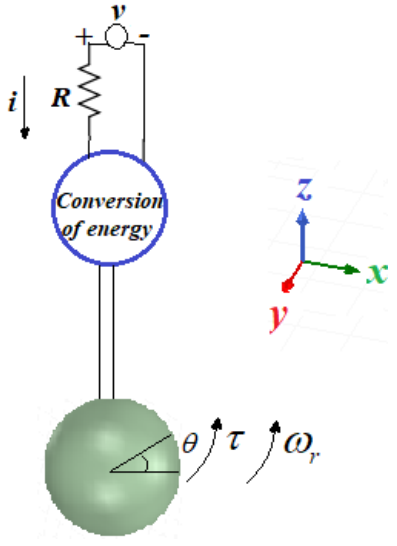

The system equation of mechanical dynamics along z-direction is given by,

$$m\frac{d^2 z}{dt^2} = mg - F_z \tag{16}$$

$$m\frac{d^2 z}{dt^2} = mg - C\left(\frac{i}{z}\right)^2$$

$$\text{where } F_z = -\frac{1}{2}i^2\frac{dL}{dz} = C\left(\frac{i}{z}\right)^2 \tag{17}$$

The system equation of mechanical dynamics along x-direction is given by,

$$m\frac{d^2 x}{dt^2} + k\frac{dx}{dt} = F_x \tag{18}$$

$$\text{or, } m\frac{d^2 x}{dt^2} = F_x - k\frac{dx}{dt}$$

$$\text{where } F(x) = -\frac{1}{2}i^2\frac{dL}{dx} = C\left(\frac{i}{x}\right)^2 \tag{19}$$

where C is the force constant, k is the air resistivity constant = 1.29, $k\frac{dx}{dt}$ is the air resistivity force and F_x is the restoring force and can be expressed as,

$$F(x) = -\frac{1}{2}i^2(b + 2cx) \tag{20}$$

a *Spherical ball:* For the spherical ball, at the nominal height of 16 mm, if small perturbation is applied from the initial point of –4 mm (Figure 8) then first it crosses the operating point of 16 mm where inductance is maximum and finally it reaches at the ending point of 1.4 mm for the 1st cycle which is shown in Figure 8(a). $\frac{dL}{dx}$ plot vs. x-direction plot is shown in Figure 8(b). At the operating point $F_x\left(-\frac{i^2}{2}\frac{dL}{dx}\right) = k\frac{dx}{dt}$ as the velocity is constant and acceleration becomes zero. $\frac{dL}{dx}$ or, F_x becomes zero at 0.2 mm after just crossing the operating point for 1st cycle. At the starting point (–4 mm), $\frac{dL}{dx}$ is initially high, then it linearly decreases and at ≈0.2 mm it becomes zero. So, at 0.2 mm, restoring force (F_x) also becomes zero [Figure 8(d)]. Corresponding current i_x vs. x-direction is shown in Figure 8(c). At the starting point where $\frac{dL}{dx}$ is high, the current is slightly less to maintain the restoring force $\left(-\frac{i^2}{2}\frac{dL}{dx}\right)$ as constant and finally it reaches the operating point where the value of current is 0.6 A which is the operating current at the nominal height. During sustained oscillation at the nominal height of 16 mm the inductance plot is shown in Figure 9(a). After 4–6 no. of cycles it finally reaches at the steady state operating position. The velocity plot is shown in Figure 9(b). At the operating point the velocity is constant, acceleration becomes zero [Figure 9(c)] and F_x becomes $k\frac{dx}{dt}$. Restoring force (F_x) becomes zero after just crossing of the operating point at 0.2 mm for 1st cycle as $\frac{dL}{dx}$ becomes zero at 0.2 mm. In the next cycle velocity reaches to 0.2 mm where the F_x became zero in the 1st cycle. At the starting and ending point of each cycle the velocity, acceleration, restoring force, air resistivity force is zero (Figure 9). At the operating point velocity is constant, acceleration is zero and restoring force (F_x) is equal to the air resistivity force ($k\frac{dx}{dt}$).

b *Flat plate 1:* For the flat plate 1, at the nominal height of 8 mm, if small perturbation is applied from the initial point of –5 mm (Figure 10) then first it crosses the operating point of 8 mm where inductance is maximum and finally it reaches at the ending point of 2.4 mm for the 1st cycle which is shown in Figure 10(a). $\frac{dL}{dx}$ plot vs. x-direction plot is shown in Figure 10(b). At the operating point $F_x\left(-\frac{i^2}{2}\frac{dL}{dx}\right) = k\frac{dx}{dt}$ as the velocity is constant and acceleration becomes zero. $\frac{dL}{dx}$ or, F_x becomes zero at 0.5 mm after just crossing the operating point for 1st cycle. At the starting point (–5 mm), $\frac{dL}{dx}$ is initially high, then it linearly decreases and at ≈0.5 mm it becomes zero. So, at 0.5 mm, restoring force (F_x) also becomes zero [Figure 10(a)]. Corresponding current i_x vs. x-direction is shown in Figure 10(c). At the starting point where $\frac{dL}{dx}$ is high, the current is slightly less to maintain the restoring force $\left(-\frac{i^2}{2}\frac{dL}{dx}\right)$ as constant and finally it reaches the operating point where the value of current is ≈0.55 A which is the operating current at the nominal height. During sustained oscillation at the nominal height of 8 mm the inductance plot is shown in Figure 11(a). After 4–6 no. of cycles it finally reaches at the steady state operating position. The velocity plot is shown in Figure 11(b). At the operating point the velocity is constant, acceleration becomes zero [Figure 11(c)] and F_x becomes $k\frac{dx}{dt}$. Restoring force (F_x) becomes zero after just crossing of the operating point at 0.5 mm for 1st cycle as $\frac{dL}{dx}$ becomes zero at 0.5 mm. In the next cycle velocity reaches to 0.5 mm where the F_x became zero in the 1st cycle. At the starting and ending

point of each cycle the velocity, acceleration, restoring force, air resistivity force is zero (Figure 11). At the operating point velocity is constant, acceleration is zero and restoring force (F_x) is equal to the air resistivity force ($k\frac{dx}{dt}$).

Figure 8 Different parameters vs. x-direction plots at the operating point for the spherical ball, (a) inductance plot for the disturbance in x-direction (b) $\frac{dL}{dx}$ plot for the disturbance in x-direction (c) current plot (i_x) for the displacement in x-direction (d) restoring force plot for the disturbance in x-direction (see online version for colours)

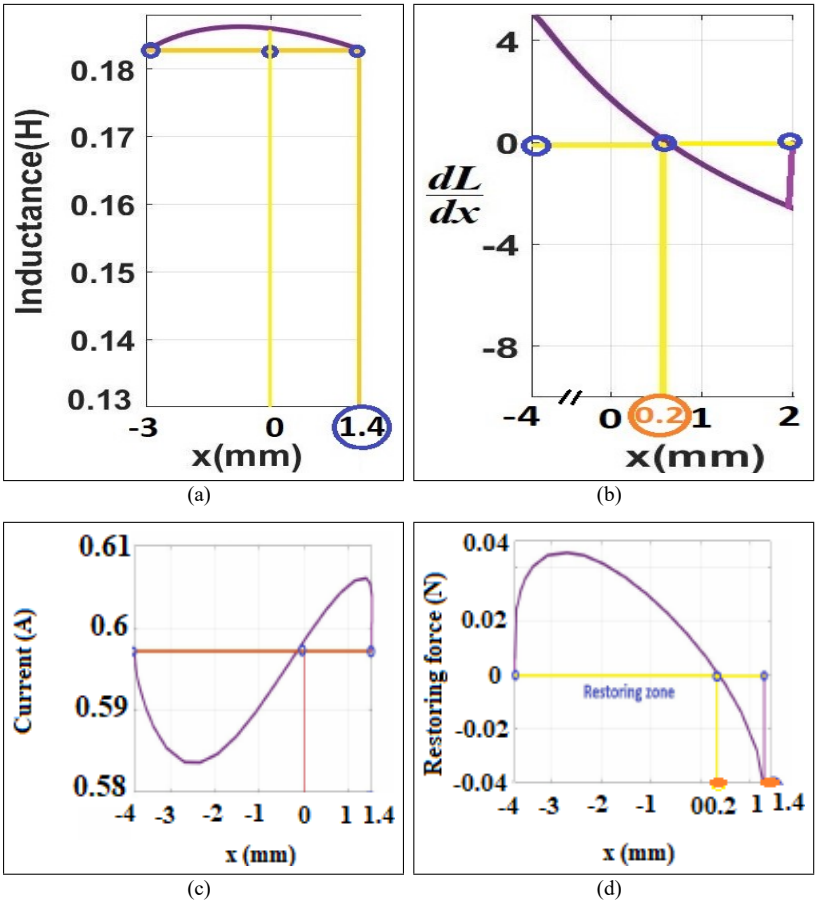

c *Flat plate 2:* For the flat plate 2, at the nominal height of 8 mm, if small perturbation is applied from the initial point of –5 mm (Table 1) then first it crosses the operating point of 8 mm where inductance is maximum and finally it reaches at the ending point of 2.6 mm for the 1st cycle which is shown in Table 1. $\frac{dL}{dx}$ or, F_x becomes zero at 0.6 mm after just crossing the operating point for 1st cycle. At the starting point (–5 mm), $\frac{dL}{dx}$ is initially high, then it linearly decreases and at ≈0.6 mm it becomes zero. So, at 0.6 mm, restoring force (F_x) also becomes zero (Table 1). At the starting point where $\frac{dL}{dx}$ is high, the current is slightly less to maintain the restoring force $\left(-\frac{i^2}{2}\frac{dL}{dx}\right)$ as constant and finally it

reaches the operating point where the value of current is 0.7 A which is the operating current at the nominal height.

Figure 9 Plots during oscillation in restoring zone for the disturbance in x-direction at the operating point for the spherical ball, (a) inductance plot during oscillation in restoring zone for the disturbance in x-direction (b) velocity plot during oscillation in restoring zone for the disturbance in x-direction (c) acceleration plot during oscillation in restoring zone for the disturbance in x-direction (d) restoring force plot during oscillation in restoring zone for the disturbance in x-direction (see online version for colours)

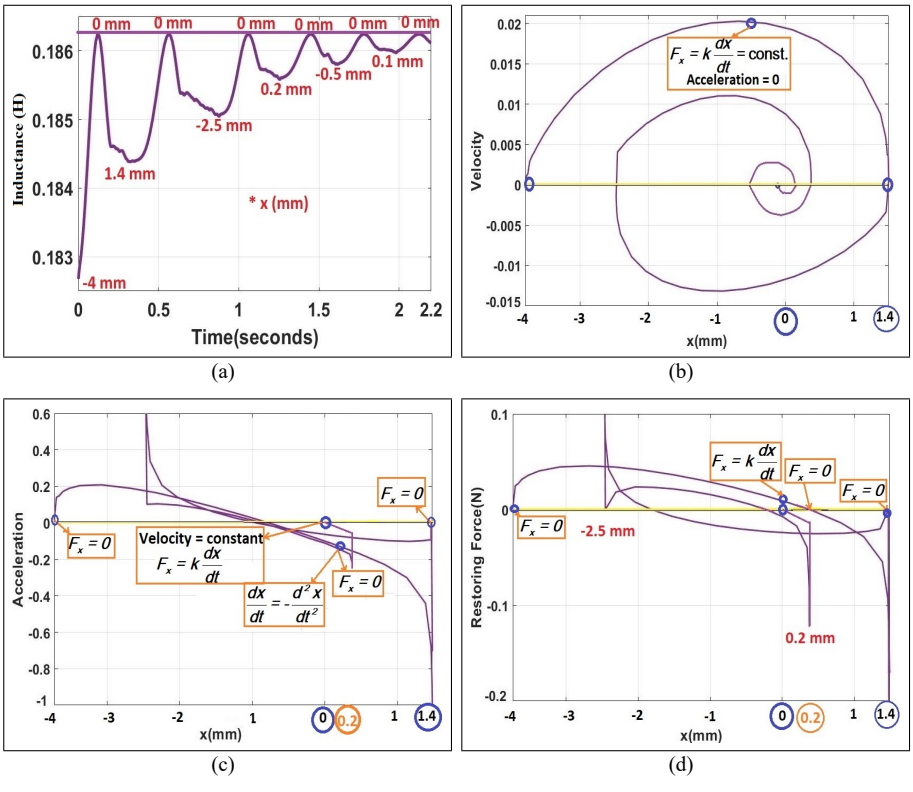

d *C-shaped plate:* For the C-shaped plate, at the nominal height of 8 mm, if small perturbation is applied from the initial point of –6 mm (Table 1)) then first it crosses the operating point of 8 mm where inductance is maximum and finally it reaches at the ending point of 3 mm for the 1st cycle which is shown in Table 1. $\frac{dL}{dx}$ or, F_x becomes zero at 0.7 mm after just crossing the operating point for 1st cycle. At the starting point (–6 mm), $\frac{dL}{dx}$ is initially high, then it linearly decreases and at ≈0.7 mm it becomes zero. So, at 0.7 mm, restoring force (F_x) also becomes zero. At the starting point where $\frac{dL}{dx}$ is high, the current is slightly less to maintain the restoring force $\left(-\frac{i^2}{2}\frac{dL}{dx}\right)$ as constant and finally it reaches the operating point where the value of current is 0.8 A which is the operating current at the nominal height.

Figure 10 Different parameters vs. x-direction plots at the nominal operating point for the flat plate 1, (a) inductance plot for the disturbance in x-direction (b) $\frac{dL}{dx}$ plot for the disturbance in x-direction (c) current plot (i_x) for the disturbance in x-direction (d) restoring force plot for the disturbance in x-direction (see online version for colours)

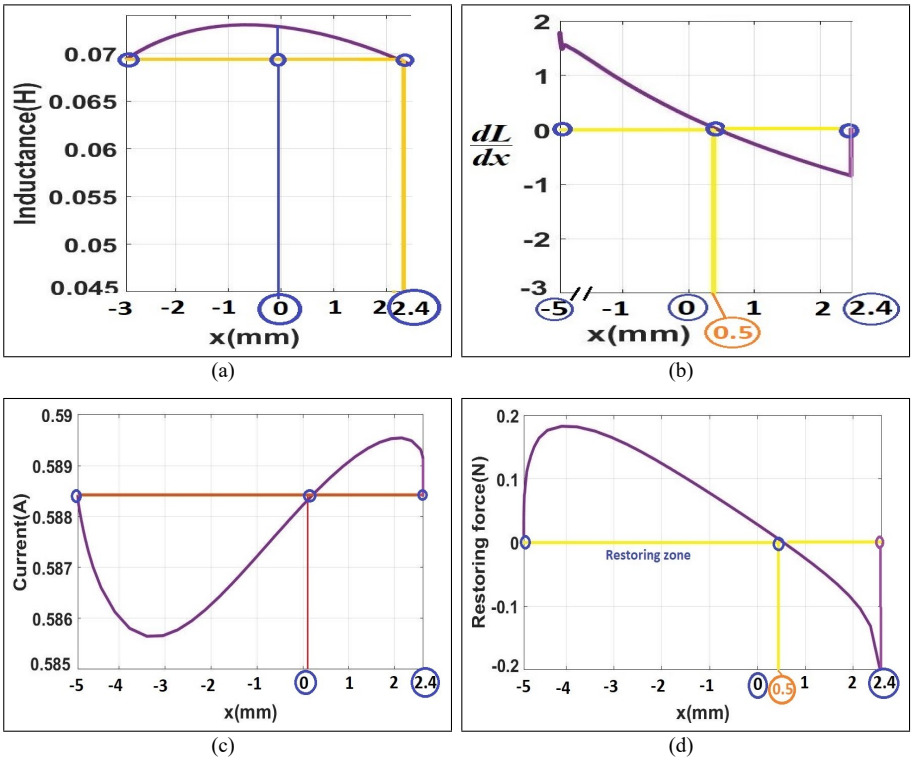

(a) (b) (c) (d)

Table 1 Dynamics in x-direction at the operating point

Disturbance in x direction			*Velocity* ($\frac{dx}{dt}$)	*Acceleration* ($\frac{d^2x}{dt^2}$)	*Air resistivity force* ($k\frac{dx}{dt}$)	*Resultant force* ($m\frac{d^2x}{dt^2}$)	*Restoring force* (F_x)
Flat plate 2	1st	–5 mm	0	0	0	0	0
	cycle	0	Constant	0	Constant	0	Constant
		0.6 mm	$\frac{dx}{dt}$	$-\frac{d^2x}{dt^2}$	$k\frac{dx}{dt}$	$-m\frac{d^2x}{dt^2}$	0
		2.6 mm	0	0	0	0	0
	2nd	2.6 mm	0	0	0	0	0
	cycle	0	Constant	0	Constant	0	Constant
		–1.1 mm	$-\frac{dx}{dt}$	$\frac{d^2x}{dt^2}$	$-k\frac{dx}{dt}$	$m\frac{d^2x}{dt^2}$	0
		–1.3 mm	0	0	0	0	0
	3rd	–1.3 mm	0	0	0	0	0
	cycle	–0.5 mm	$\frac{dx}{dt}$	$-\frac{d^2x}{dt^2}$	$k\frac{dx}{dt}$	$-m\frac{d^2x}{dt^2}$	0
		0	Constant	0	Constant	0	Constant
		0.5 mm	0	0	0	0	0
	4th	0.5 mm	0	0	0	0	0
	cycle	0	Constant	0	Constant	0	Constant
		–0.2 mm	$-\frac{dx}{dt}$	$\frac{d^2x}{dt^2}$	$-k\frac{dx}{dt}$	$m\frac{d^2x}{dt^2}$	0
		–0.4 mm	0	0	0	0	0

Table 1 Dynamics in x-direction at the operating point (continued)

Disturbance in x direction			*Velocity* $(\frac{dx}{dt})$	*Acceleration* $(\frac{d^2x}{dt^2})$	*Air resistivity force* $(k\frac{dx}{dt})$	*Resultant force* $(m\frac{d^2x}{dt^2})$	*Restoring force* (F_x)
C-shaped plate	1st cycle	–6 mm	0	0	0	0	0
		0	Constant	0	Constant	0	Constant
		0.7 mm	$\frac{dx}{dt}$	$-\frac{d^2x}{dt^2}$	$k\frac{dx}{dt}$	$-m\frac{d^2x}{dt^2}$	0
		3 mm	0	0	0	0	0
	2nd cycle	3 mm	0	0	0	0	0
		0	Constant	0	Constant	0	Constant
		–0.9 mm	$-\frac{dx}{dt}$	$\frac{d^2x}{dt^2}$	$-k\frac{dx}{dt}$	$m\frac{d^2x}{dt^2}$	0
		–1.9 mm	0	0	0	0	0
	3rd cycle	–1.9 mm	0	0	0	0	0
		–0.2 mm	$\frac{dx}{dt}$	$-\frac{d^2x}{dt^2}$	$k\frac{dx}{dt}$	$-m\frac{d^2x}{dt^2}$	0
		0	Constant	0	Constant	0	Constant
		0.7 mm	0	0	0	0	0
	4th cycle	0.7 mm	0	0	0	0	0
		0	Constant	0	Constant	0	Constant
		–0.05 mm	$-\frac{dx}{dt}$	$\frac{d^2x}{dt^2}$	$-k\frac{dx}{dt}$	$m\frac{d^2x}{dt^2}$	0
		–0.1 mm	0	0	0	0	0

Figure 11 Plots during oscillation in restoring zone for the disturbance in x-direction at the operating point for the flat plate 1, (a) inductance plot during oscillation in restoring zone for the disturbance in x-direction (b) velocity plot during oscillation in restoring zone for the disturbance in x-direction (c) acceleration plot during oscillation in restoring zone for the disturbance in x-direction (d) restoring force plot during oscillation in restoring zone for the disturbance in x-direction (see online version for colours)

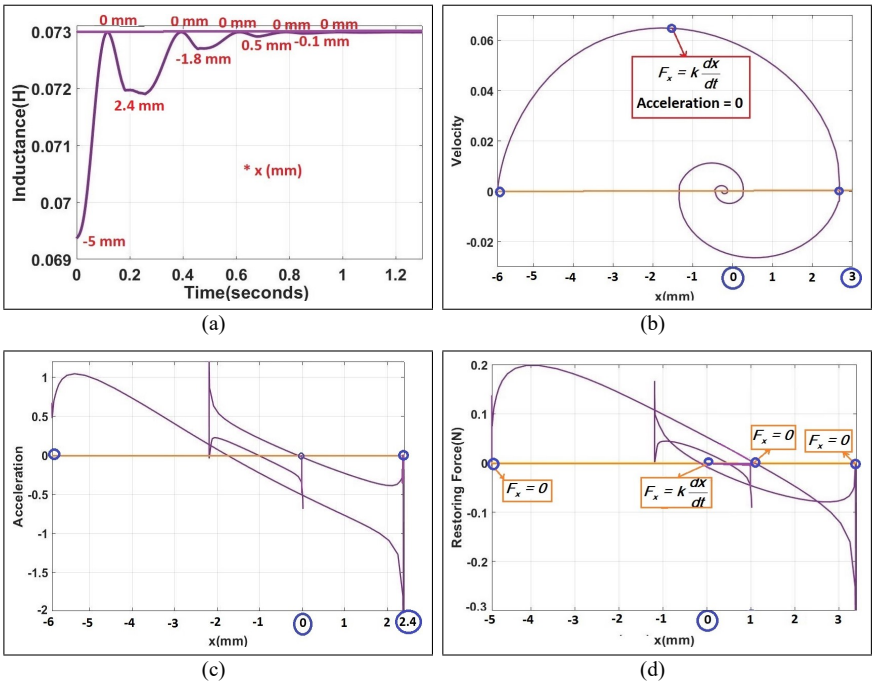

Figure 12 Inductance plot during oscillation in restoring zone for the disturbance in x-direction at the nominal operating point, (a) inductance plot during oscillation in restoring zone for the disturbance in x-direction for the spherical ball (b) inductance plot during oscillation in restoring zone for the disturbance in x-direction for the flat plate 1 (c) inductance plot during oscillation in restoring zone for the disturbance in x-direction for the flat plate 2 (d) inductance plot during oscillation in restoring zone for the disturbance in x-direction C-shaped plate (see online version for colours)

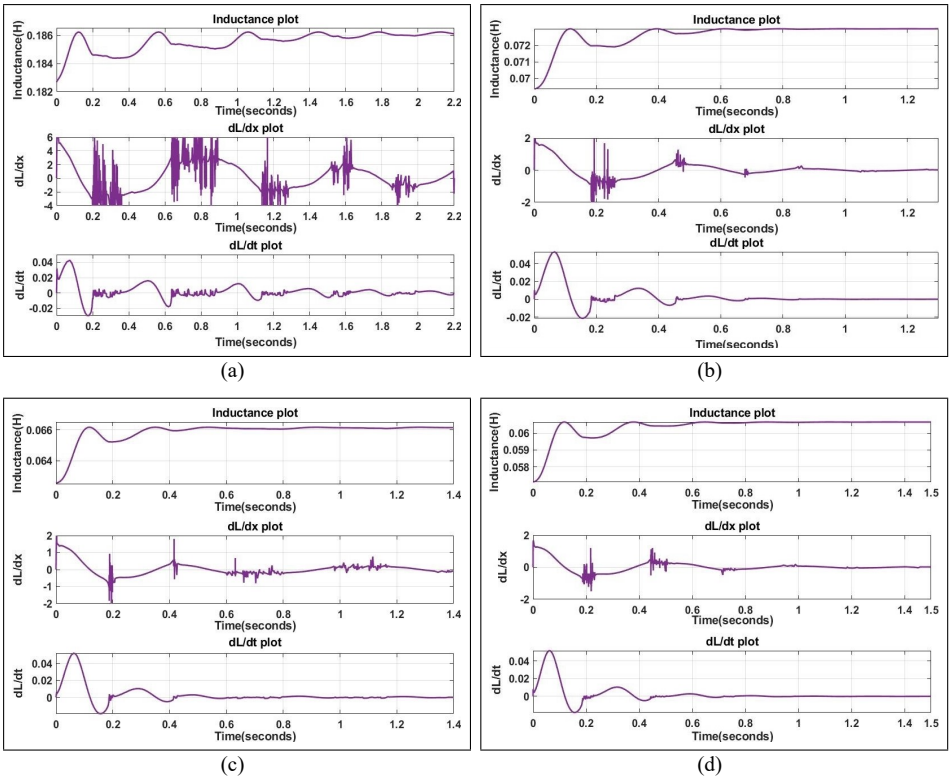

4 System modelling in transverse direction

The voltage across the EM coil can be written as,

$$v = Ri + L\frac{di}{dt} + i\frac{dL}{dt} \tag{21}$$

$$\text{or, } v = Ri + L\frac{di}{dt} + i\frac{\delta L}{\delta z}\frac{dz}{dt} + i\frac{\delta L}{\delta x}\frac{dx}{dt} \tag{22}$$

$$\text{or, } v = Ri + L(x,z)\frac{di}{dt} + i\frac{\delta L}{\delta x}v_x + i\frac{\delta L}{\delta z}v_z \tag{23}$$

In case of x-direction modelling, the velocity in z-direction (v_z) at the operating point is zero. Therefore the above equation can be written as,

$$v = Ri + L\frac{di}{dt} + i\left(\frac{\delta L}{\delta x}v_x\right) \tag{24}$$

Applying small perturbation around the operating point it can be written as,

$$\begin{aligned} v_0 + \Delta v_0 = {} & R(i_0 + \Delta i_0) + (L_0 + \Delta L_0)\frac{d(i_0 + \Delta i_0)}{dt} \\ & + (i_0 + \Delta i_0)\Big[\frac{\delta(L_0 + \Delta L_0)}{\delta z_0}\frac{d(z_0 + \Delta z_0)}{dt}\Big] \\ & + (i_0 + \Delta i_0)\Big[\frac{\delta(L_0 + \Delta L_0)}{\delta x_0}\frac{d(x_0 + \Delta x_0)}{dt}\Big] \end{aligned}$$

where $x - x_0 = \Delta x_0$, $i - i_0 = \Delta i_0$.

Now the small perturbation model becomes,

$$\Delta v_0 = R(\Delta i_0) + L_0\frac{d(\Delta i_0)}{dt} + (\Delta i_0)\Big[\frac{\delta L_0}{\delta x} \times \frac{d(\Delta x_0)}{dt}\Big] \tag{25}$$

The system equation of mechanical dynamics along x-direction is given by,

$$m\frac{d^2x}{dt^2} + k\frac{dx}{dt} = F_x$$

$$\text{or, } m\frac{d^2x}{dt^2} = F_x - k\frac{dx}{dt} \tag{26}$$

$$\text{where } F_x = -\frac{1}{2}i^2\frac{dL}{dx} \tag{27}$$

$$F_x = -\frac{1}{2}i^2\frac{dL}{dx} = C\Big(\frac{i}{x}\Big)^2 \tag{28}$$

Applying small perturbation around the operating point (i_0, x_0) the equation can be written as,

$$F(i,x) = F(i_0,x_0) + (i - i_0)\frac{dF}{di} + (x - x_0)\frac{dF}{dx}$$

$$\text{or, } F_x = F(i_0,x_0) + \Delta i\frac{dF}{di} + \Delta x\frac{dF}{dx} \tag{29}$$

After small perturbation at the operating point of (i_0, x_0), the mechanical equation (26) can be written as,

$$m\frac{d^2\Delta x_0}{dt^2} = \Delta i_0\frac{dF}{di} + \Delta x_0\frac{dF}{dx} - k\frac{d\Delta x_0}{dt} \tag{30}$$

$$\text{where } \frac{dF}{di} = K_{i_0} = \frac{2Ci_0}{x_0} \tag{31}$$

$$\frac{dF}{dx} = K_{x_0} = \frac{2Ci_0^2}{x_0^3} \tag{32}$$

$$m\frac{d^2\Delta x_0}{dt^2} = \Delta i_0\Big(\frac{2Ci_0}{x_0}\Big) - \Delta x_0\Big(\frac{2Ci_0^2}{x_0^3}\Big) - \Big(k\frac{\Delta x_0}{dt}\Big)$$

$$m\frac{d^2\Delta x_0}{dt^2} = K_{i_0}\Delta i_0 - K_{x_0}\Delta x_0 - k\frac{\Delta x_0}{dt}$$

$$m\frac{d^2\Delta x_0}{dt^2} + k\frac{\Delta x_0}{dt} = K_{i_0}\Delta i_0 - K_{x_0}\Delta x_0 \tag{33}$$

Taking Laplace transform the expression can be written as,

$$ms^2\Delta X_0(s) + ks\Delta X_0(s) = K_{i_0}\Delta I_0(s) - K_{x_0}\Delta X_0(s)$$
$$\frac{\Delta X_0(s)}{\Delta I_0(s)} = \frac{K_{i_0}}{(ms^2 + ks + K_{x_0})} \tag{34}$$

During sustained oscillation in restoring zone the inductance plot is shown in Figure 11(a). The velocity plot during sustained oscillation for the displacement in x-direction at the operating point is shown in Figure 11(b) where velocity becomes zero at the operating point. Acceleration plot also shows that after few cycle of oscillation the acceleration becomes zero [Figure 11(c)] at the operating point. So the system become stable for small disturbance in x-direction due to restoring zone exists (Figure 11).

Figure 13 Lateral displacement of flat plate 2 at the nominal operating height, (a) flat plate with displacemnt of –10 mm (b) flat plate with displacement of 10 mm (c) flat plate with displacement of –30 mm (d) flat plate with displacement of 30 mm (see online version for colours)

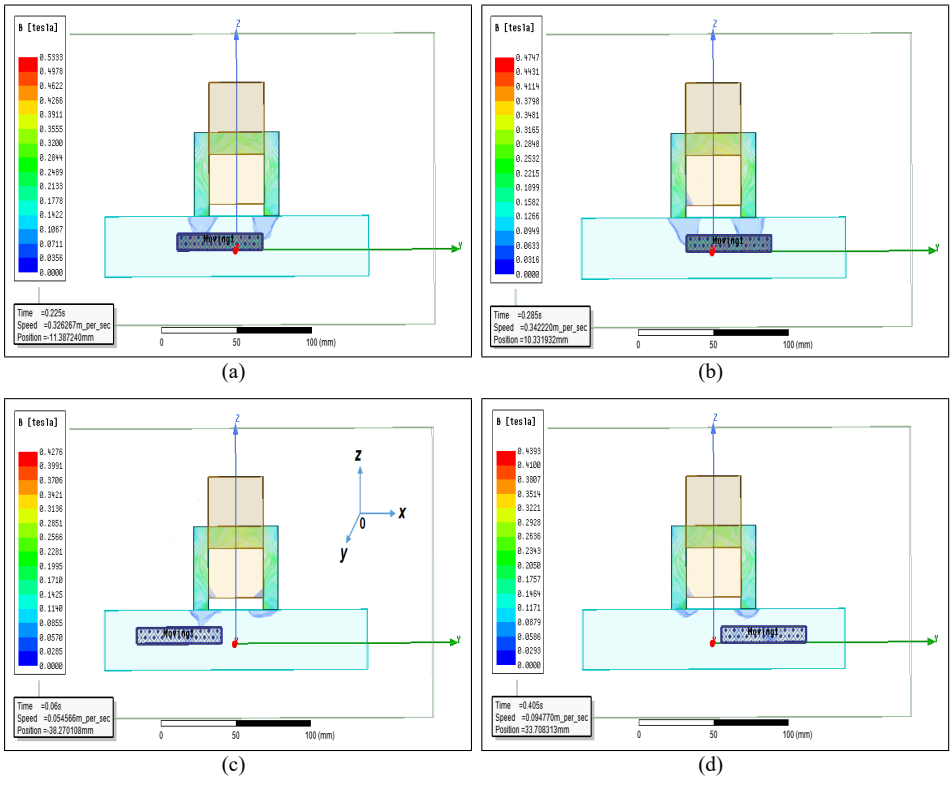

(a) (b) (c) (d)

It is observed from *FEM* analysis [Figures 13(a) and 13(b)] that the electromagnetic restoring energy will readjust the flux lines with the position of the plate as the flux lines generated by the limb of the core crosses the ferromagnetic plate (displacement of 10 mm along x-direction) whereas at ± 30 mm displacement [Figures 13(c) and 13(d)] the flux lines generated by the limb can not link with the ferromagnetic plate. So the *EM* restoring force will be minimal and the possibility of restoration is least. Additionally, for the C-shaped plate, the leakage flux is more compared to the flat plate as observed in Figures 13(b) and 14(b).

Table 2 Desired and practical values of operating position and current during stable levitation

Objects	*Operating gap (z_0)*		*Operating current (i_0)*	
Spherical object	Predicted 16 mm	Practical 13 mm	Predicted 0.6 A	Practical 0.45 A
Rectangular steel plate 1	Predicted 8 mm	Practical 7 mm	Predicted 0.55 A	Practical 0.43 A
Rectangular steel plate 2	Predicted 8 mm	Practical 7 mm	Predicted 0.7 A	Practical 0.64 A
C-shaped plate	Predicted 8 mm	Practical 7 mm	Predicted 0.8 A	Practical 0.7 A

Table 3 Levitation prototype specifications

Parameters		*Spherical ball (62 gm)*	*Flat plate 1 (65 gm)*	*Flat plate 2 (148 gm)*	*C-shaped plate (148 gm)*
Mass	m	62 gm	65 m	148 gm	148 gm
Levitating force	F	0.6 N	0.65 N	1.46 N	1.46 N
Gap	z_0	16 mm	8 mm	8 mm	8 mm
Coil current	i_0	0.61 A	0.55 A	0.7 A	0.81 A
Coil inductance	L_{coil}			0.02 H	0.02 H
Inductance	L_{z_0}	0.49 H	0.063 H	0.06 H	0.05 H
Extra inductance by the ferromagnetic steel object	L_0	0.2 H	0.04 H	0.043 H	0.03 H
The force constant	C (analytical)	7.95×10^{-5} H-m	1.72×10^{-4} H-m	1.72×10^{-4} H-m	1.22×10^{-4} H-m
Force constant	C (practical)			1.9×10^{-4} H-m	1.43×10^{-4} H-m
EM-coil resistance	R	32 Ω	11 Ω	11 Ω	11 Ω
Sensitivity of the sensor	B	1.36 V/mm	1 V/mm	1 V/mm	1 V/mm
DC gain of the system	K	5.58	46	25	23
Mechanical dynamics	$G_1(s)$	$\frac{5.58}{(s+14.5)(s-14.5)}$	$\frac{46}{(s+56)(s-56)}$	$\frac{25}{(s+46)(s-46)}$	$\frac{23}{(s+48)(s-48)}$
Electrical dynamics	$G_2(s)$	$\frac{1}{(32+0.49s)}$	$\frac{1}{(11+0.0.06s)}$	$\frac{1}{(11+0.06s)}$	$\frac{1}{(11+0.05s)}$
Position controller (lead compensator)	$C_1(s)$	$\frac{21(s+10)}{(s+100)}$	$\frac{8(s+50)}{(s+550)}$	$\frac{4(s+45)}{(s+450)}$	$\frac{4(s+45)}{(s+450)}$
Current controller (PI)	$C_2(s)$	nil	$\frac{8(s+450)}{s}$	$\frac{9.4(s+657)}{s}$	$\frac{7.5(s+725)}{s}$
Open loop poles of the system		–65, –14, +14	–183, –56, +56	–183, –47, +47	–174, –49, +49
Closed loop poles of the system		–12 ± i41, –133, –7	–50+i, –100 ± i3, –201+i, –600+i	-310 ± i425, –400, –60, –13	–288 ± i408, –411, –57, –25
GM of the system		66.7 dB	62.7 dB	56.4 dB	57.9 dB

5 Summary

The system dynamics of electromagnetic levitation system for the disturbance in x-direction of four different shaped objects has been broadly investigated in this work. Velocity and acceleration plot in the restoring zone has been observed closely at the operating point (Figures 9 and 11). The above study shows that operating zone is larger for the C-shaped plate during sustained oscillation (–6 mm). So, from this study e can comment on stability itself. The stability is best for the spherical symmetrical object. Also the stability is better for the C-shaped object compared to a same mass of a flat object. The comparative study is claimed as a substantial addition to attraction type electromagnetic levitation practical applications (Tables 2 and 3). This work will allow the designer to compute the model geometric dimensions with greater accuracy than allowed by the approaches found in the available published literatures. In real life applications geometric discontinuity is a major concern. The effects of disturbances on performance along the transverse direction for these symmetric and asymmetric objects have been broadly investigated in this work and has been compared with a symmetric shaped object which may help the asymmetric discontinuity problems in real life electromagnetic levitation applications.

Figure 14 Lateral displacement of C-shaped plate at the nominal operating height, (a) C-shaped plate with no displacement along horizontal direction (b) C-shaped plate with displacement of 10 mm (see online version for colours)

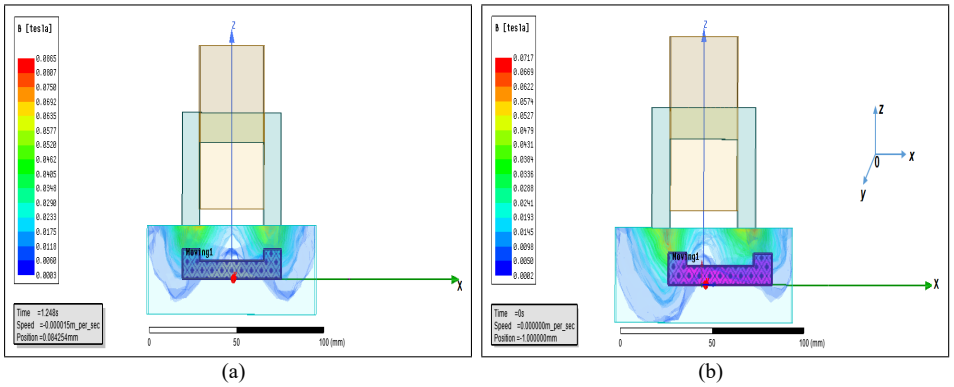

(a) (b)

References

Banerjee, S. and Bhaduri, R. (2010) 'Two actuator based dc attraction type levitation system for the suspension of a cylindrical rod', *IET Elect. Power Appl.*, Vol. 5, No. 9, pp.721–730.

Banerjee, S., Kumar, T.K.S., Pal, J. and Prasad, D. (2008) 'Controller design for large-gap control of electromagnetically levitated system by using an optimization technique', *IEEE Trans. Control Systems Technology*, May, Vol. 16, No. 3, pp.408–415.

Bittar, A., Cruz, J. and Sales, R. (1998) 'A new approach to the levitation control of an electromagnetic suspension vehicle', in *Proc. of IEEE Int. Conf. on Control Applications*, Vol. 272, Nos. 3–5, pp.263–270.

Chen, J. and Tsukamoto, O. (1991) 'Attractive type magnetic levitation system with 3 ac electro-magnets', in *Proc. IEEE Int. Conf. IECON*, November, Vol. 1, pp.778–782.

Debnath, S., Biswas, P.K. and Das, U. (2018) 'Analysis and simulation of different types of power amplifiers used in electromagnetic levitation system', *Journal of Power Technologies*, Vol. 98, No. 2.

Jayawant, B.V. (1988) 'Review lecture on electromagnetic suspension and levitation techniques', *in Proc. R. Soc. Lond.*, Vol. 416, pp.245–320.

Jia, Y., Zhao, P., Xie, J., Zhang, X., Zhou, H. and Fu, J. (2021) 'Single-electromagnet levitation for density measurement and defect detection', *Frontiers of Mechanical Engineering*, Vol. 16, No. 1, pp.186–195.

Jinhui, L., Jie, L., Danfeng, Z., Peng, C., Lianchun, W. and Peichang, Y. (2015) 'The active control of maglev stationary self-excited vibration with a virtual energy harvester', *IEEE Transactions on Industrial Electronics*, May, Vol. 62, No. 5, pp.2942–2951.

Jo, J., Han, Y., Lee, C., Kang, B.K.K., Nam, Y., Park, S. and Lee, S. (2010) 'Design and control of the miniature maglev using electromagnets and permanent magnets in magnetic levitation system', *International Conference on Control, Automation and Systems*, KINTEX, Gyeonggi-do, South Korea, October, pp.27–30.

Kumar, D., Sisodiya, M.S. and Bajpai, V. (2022) 'A novel servo-stabilized electromagnetic levitation for micro-EDM processing and its feasibility analysis', *Proceedings of the Institution of Mechanical Engineers, Part B: Journal of Engineering Manufacture*, p.9544054221124473.

Kundu, J. and Sengupta, M. (2015) 'Design, modelling, fabrication of a single-axis attraction type levitation prototype with 3-degree freedom control', in *Proc. Natl. Conf. NPEC*, IIT Bombay.

Kundu, J., Sengupta, M. and Sengupta, A. (2013) 'Design, modelling, fabrication and testing of an electromagnetic coil system for a levitation mechanism', in *Proc. Natl. Conf. NPEC*, December.

Kundu, J., Sengupta, M. and Sengupta, A. (2014) 'Design, modelling, fabrication and control of an attraction type levitation prototype', in *Proc. IEEE Intl. Conf.*, IIT Bombay, PEDES.

Ma, G., Wang, Z., Liu, K., Qian, H. and Wang, C. (2018) 'Potentials of an integrated levitation, guidance, and propulsion system by a superconducting transverse flux linear motor', *IEEE Transactions on Industrial Electronics*, September, Vol. 65, No. 9, pp.7548–7557.

Matsumura, F. and Yamada, S. (1974) 'A method to control the suspension system utilizing magnetic attractive force', in *Proc. Elect. Engg.*, Vol. 94, pp.50–54.

Mofushita, M., Azukizawa, T., Kanda, S. and Tamura, T.Y.N. (1989) 'A new maglev system for magnetically levitated carrier system', *IEEE Transactions on Vehicular Technology*, Vol. 38, No. 4, pp.230–236.

Moon, F.C. (1994) *Superconducting Levitation, Applications to Bearings and Magnetic Transportation*, John Wiley and Sons, USA.

Morishita, M. and Azukizawa, T. (1988) 'Zero power control method for electromagnetic levitation system', *IEEE Proc.*, Vol. 108, No. 45, pp.447–451.

Ohtsuka, T. and Kyotani, Y. (1975) 'Superconducting levitated high speed ground transportation project in Japan', *IEEE Transactions on Magnetics*, March, Vol. MAG-11, No. 2, pp.608–614.

Pal, J., Prasad, D. and Banerjee, S. (2002) 'A unifying approach for development of magnetically suspended vehicle using controlled dc electromagnet', in *Proc. Int. Conf. IEEE-ACE (EPIC)*, pp.404–408.

Rogg, D. (1984) 'General survey of the possible applications and development tendencies of magnetic levitation technology', *IEEE Trans. Magnetics*, September, Vol. 20, pp.1696–1701.

Sengupta, M. and Sengupta, A. (2001) 'Design, implementation and testing of an attraction type magnetic levitation system', in *Proc. Int. Conf. EAIT*, December, pp.17–20.

Sinha, P.K. (1987) *Electromagnetic Suspension: Dynamics and Control*, Peter Peregrinus, London, UK.

Sun, Y., Li, W., Xu, J., Qiang, H. and Chen, C. (2017) 'Nonlinear dynamic modeling and fuzzy sliding-mode controlling of electromagnetic levitation system of low-speed maglev train', *Journal of Vibroengineering*, Vol. 19, No. 1, pp.328–342.

Sun, Y-G., Xu, J-Q., Chen, C. and Lin, G-B. (2019) 'Fuzzy H_∞ robust control for magnetic levitation system of maglev vehicles based on ts fuzzy model: design and experiments', *Journal of Intelligent & Fuzzy Systems*, Vol. 36, No. 2, pp.911–922.

Venkataratnam, K., Bhattacharya, T.K. and Sengupta, M. (1998) 'Theory, performance prediction and indirect sensing of rotor position in a switched reluctance motor under bulk saturation', *IEEE Proc. EPA*, November.

Wang, Z., Long, Z. and Li, X. (2018) 'Levitation control of permanent magnet electromagnetic hybrid suspension maglev train', *Proceedings of the Institution of Mechanical Engineers, Part I: Journal of Systems and Control Engineering*, Vol. 232, No. 3, pp.315–323.

Wang, D., Li, X., Liang, L. and Qiu, X. (2020) 'Dynamic interaction analysis of bridges induced by a low-to-medium – speed maglev train', *Journal of Vibration and Control*, Vol. 26, Nos. 21–22, pp.2013–2025.

Wong, T.H. (1986) 'Design of a magnetic levitation control system', *IEEE Trans. Educ.*, November, Vol. E-29, No. 4, pp.196–200.

Xu, J., Leng, Y., Sun, F., Su, X. and Chen, X. (2022) 'Modeling and performance evaluation of a bi-stable electromagnetic energy harvester with tri-magnet levitation structure', *Sensors and Actuators A: Physical*, Vol. 346, No. 5, p.113828.

Yamamura, S. and Yamaguchi, H. (1990) 'Electromagnetic levitation system by means of salient-pole type magnets coupled with laminated slotless rails', *IEEE Trans. Vehicular Tech.*, February, Vol. 39, pp.83–88.